Mohammadzadehmoghadam, S. and Dong, Y. and Davies, I. 2016. Modeling electrospun nanofibers: An overview from theoretical, empirical, and numerical approaches. International Journal of Polymeric Materials and Polymeric Biomaterials. 65 (17): pp. 901-915.

Modelling Electrospun Nanofibres: An overview from theoretical, empirical to numerical approaches

Soheila Mohammadzadehmoghadam, Yu Dong*, Ian Jeffery Davies

Department of Mechanical Engineering, Curtin University, Perth, WA 6845, Australia

Abstract

Electrospinning is a sophisticated material process to manufacture well-tailored nanofibres for fibre reinforcement, tissue scaffolding, drug delivery, nanofiltration, cosmetics, protective clothing, *etc*. Abundant information and knowledge are reported from experimental observation and material characterisation to determine and control nanofibre properties. However, experimental results need to be interpreted systematically through theoretical, analytical and numerical models for the optimisation of fibre diameter and alignment, porosity, and estimation of mechanical properties of electrospun nanofibres. This paper provides a comprehensive review on current status of modelling approaches used in electrospun nanofibres to elucidate their systematic research approaches from material fabrication, experimental characterisation to modelling.

Keywords: Electrospinning, nanofibres, modelling, fibre diameter, porosity, permeability, mechanical properties.

* Corresponding author. Tel.: +61 8 92669055; fax: +61 8 92662681.
E-mail address: Y.Dong@curtin.edu.au (Y. Dong).

1. Introduction

Electrospinning is a simple and straightforward polymer processing method for fabricating ultrathin polymeric fibres with diameters ranging from 20 nm to 20 μm. The use of electrospun fibres for various applications has been well documented in the literature due to their small fibre diameter and porous structure [1-3]. In each of their applications, the control of fibre diameter is essential to achieve specific functionalities to structural networks and increase their available surface areas [4-6]. Moreover, mechanical properties of electrospun fibres in relation to their diameters have been well established [7, 8]. Other features widely discussed are their porous structure and permeability that are required for particular applications such as engineering tissue scaffolds [9]. Finally, mechanical properties of such fibrous materials are critical to their success in further applications. For instance, the stiffness of artificial substrates based on these materials is known to influence cell growth, proliferation and differentiation in tissue engineering. On the other hand, strength and durability are required for different applications such as filtration, protective clothing and fabrics [10, 11]. Consequently, the control of fibre diameter and morphology, size and distribution of pores, as well as evaluation of mechanical properties of electrospun fibrous materials by means of quantitative study and modelling approaches are beneficial to material researchers and engineers in order to achieve desirable properties and fulfil application requirements.

2. Electrospinning

Strictly speaking, fibres with diameters of less than approximately 100 nm are referred to as nanofibres within the scientific literature. Currently, nanofibre fabrication is one of key advancements in nanotechnology and nanomanufacturing. Among various approaches for producing polymeric nanofibres [12-16], electrospinning or electrostatic spinning is recognised as the cheapest and most straightforward bench-top technique for fabricating continuous nanofibres with diameters ranging from several micrometers down to tens of nanometers. The

technique is particularly promising and versatile since it facilitates the production of multifunctional nanofibres from a variety of polymers, polymer blends, sol–gels, composites and ceramics [17-19].

Studies on electrically driven liquid jets were initially introduced by Cooley [20] and Morton [21] in 1902. Several years later, Formhals [22] contributed to the development of electrospinning and filed several patents on innovative technology related to the topic. However, it has only been since the early 1990s that the popularity of electrospinning has increased significantly with more than a hundred electrospinnable synthetic and natural polymers investigated [23].

The basic framework of electrospinning is shown in Fig. 1. Firstly, polymer melt or solution is introduced into a capillary tube with a high electrical potential applied between droplets of polymer solution or melts at the end of a metallic needle and a grounded collector. When increasing the intensity of electric field, pendant drop of polymer solution becomes highly electrified and an electric charge is induced on the liquid surface. As a result, liquid drops are deformed into a conical shape to form a well-known Taylor cone. When the electric voltage reaches a critical value, electrostatic repulsion forces prevail over solution surface tension so that a charged jet of solution is ejected. During its trajectory, the jet becomes considerably elongated and deformed into a spiral shape whilst the solvent simultaneously evaporates within milliseconds until it reaches the collector. During this process, the jet also undergoes three types of instabilities, namely Rayleigh instability, bending instability and whipping instability [23-26].

Electrospinning is a complex process that involves solvent diffusion/evaporation/cooling, heat transfer, water condensing, and polymer diffusion in addition to operation variables [28]. This process can be categorised into several stages such as jet initiation [29], steady-state jet motion, [30, 31], jet instabilities [32], solidification into nanofibres [33] and nanofibre

deposition. The first detailed mathematical study on the subject of electrified fluid jet was undertaken in 1960s with the introduction of the “Leaky Dielectric Model” [34, 35]. Later on, important progress has been made in understanding the electrospinning process, and several theoretical models have been proposed to specifically treat one or two aforementioned individual stages of the process. Interested readers can find more details regarding modelling of electrospinning process elsewhere [36, 37].

3. Role of Diameter on the Mechanical Behaviour of Electrospun Nanofibres and Their Applications

It has been shown that fibre diameter has a direct effect on mechanical properties of electrospun nanofibres (Fig. 2). Pai *et al.* [38] investigated Young’s moduli and yield strengths of individual electrospun poly(trimethyl hexamethylene terephthalamide) (PA 6(3)T) polymeric fibres under uniaxial tension with both properties increasing with decreasing fibre diameter (less than 500 nm). This trend has also been reported for other electrospun nanofibres in previous literatures [39-44].

Several factors may contribute to the size-effect of nanofibres. Wu and Dzenis [45, 46] and other groups [47, 48] modelled the size effect of polymer nanofibres by considering the surface energy to contribute to axial tensile force based on continuum mechanics. It is assumed that fibres with different sizes are isotropic and have identical fibre morphology. However, this hypothesis is insufficient to interpret such fibre behaviour when it is below critical fibre diameter where size dependency is observed. Therefore, other potential factors are required to be considered [45]. This behaviour was also ascribed to an increase in the degree of crystallinity and a gradual ordering of microstructure as a function of fibre diameter during electrospinning [43,44,49,50]; whereas other studies have reported a minor increase [8,51] or even decrease [52] in the crystallinity of electrospun nanofibres as a function of their diameter, which does not agree with this assumption.

Ji *et al.* [53] proposed a model in which the combination of large shear imposed during the electrospinning process and surface tension resulted in a higher number of monomers to be aligned on the fibre surface and in contact with the surface. By reducing the fibre diameter, polymeric chains could span along both surfaces so that opposite sides of fibres became physically coupled in order to further reinforce fibres. Stachewicz *et al.* [51] suggested a composite model of an anisotropic shell surrounding an isotropic core in order to understand the increase in elastic modulus with decreasing fibre diameter. This core-shell model was supported by using phase imaging for the cross-section of an individual electrospun polyvinyl alcohol (PVA) fibre based on atomic force microscopy (AFM), as illustrated in Fig. 3a. The shell thickness remained fairly constant at approximately 30 nm (Fig. 3b), signifying that the relative contribution of the shell increased with decreasing fibre diameter, thus resulting in an enhanced fibre elastic modulus. Further, Baji *et al.* [54] used transmission electron microscopy (TEM) to visualise the microstructures of fibres and investigate the effect of fibre size on fibre morphology. As shown in Fig. 4, polyvinylidene fluoride (PVDF) nanofibres with a diameter of 70 nm revealed a typical skin-core structure in their fibre morphology.

According to Curgul *et al.* [55], mechanical deformation of fibres is affected by their skin-core morphology. The mass density in the core region is similar to that of bulk polymer, and thus the core region of fibres exhibits bulk-like structure and physical properties. In contrast, the properties exhibited by the surface region are totally different, which is ascribed to significantly lower density and increased chain mobility at the fibre surface/skin when compared to the core region. Camposeo *et al.* [56] correlated the internal structure of an electrospun functional nanofibre with its local stiffness. Such experiments directly revealed that polymeric nanofibres comprise a dense internal core embedded in a less dense polymeric shell. Additionally, the dense core is twice as stiff as the polymeric shell. Measurements using scanning near-field optical microscopy (SNOM) indicated higher optical absorption at the fibre

centre and lower absorption closer to its boundary, signifying higher polymer concentration at the fibre core.

Arinsten *et al.* [8, 57] suggested a model based on the concept of supramolecular structure with an amorphous phase, consisting of oriented fragments of polymer chains. Nanofibres can then be considered as a ‘‘composite’’ with supramolecular structures (ellipsoid-like regions) as effective ‘‘anisotropic particles’’. Their long axis is partially oriented along the fibre axis, surrounded and separated by a binder (*i.e.* thin amorphous polymer layers). When nanofibres are subjected to a longitudinal stress, elongation is accompanied by relative rotation of supramolecular structures, thus decreasing their tilt angle with respect to the fibre axis. The confinement effect is given by the fact that these rotations are hindered by the fibre boundary and surface acting as a wall. As a result, the elastic modulus inevitably depends on fibre diameter. This restriction is dominant for thin fibres, but it becomes negligible for thick fibres [57]. A molecular-based hyperelastic model to simulate size-dependent mechanical properties of polymer nanostructures was developed by Tang *et al.* [58]. Instead of using surface tension to describe the size effect in nanofibres, a higher degree of constraints for polymer motion is assumed on the surface when compared to the core of nanofibres. The continuum model predicts size effects in polymeric nanostructures based on various polymer constraints between the skin and core. Recently, Yuan *et al.* [59] presented a higher-order strain gradient (HSGE) model, which introduced the second gradient of the strain into a deformation energy model to capture the size dependency on nanofibres. It is hypothesised that nanofibres are elastic, isotropic and uniform with good agreement between experimental data and predicted modelling results obtained.

Another interesting phenomenon that has been observed is known as surface rippling or wrinkling when electrospun nanofibres undergo axial stretching. Such behaviour was first detected by Naraghi *et al.* [60] when studying the deformation process of polyacrylonitrile

(PAN) nanofibres by microelectromechanical systems (MEMS)-based micro tension tests. A cascade of periodical ripples (necks) has been found on the surface of these nanofibres at the two largest rates (Fig. 5); whereas at lower strain rates, nanofibres are deformed homogeneously without a sign of surface ripples. These ripples were also observed within as-electrospun polyimide (PI) nanofibres after imidisation in the nitrogen environment at approximately 400°C. In this case, the rippling formation may be related to axial shrinking induced in the imidisation process [45]. In principle, the formation of ripples on the surface of electrospun nanofibres offers a surface instability phenomenon that can greatly affect their performance by acting as a failure mechanism or even by extending their applications through controlling this phenomenon [61]. Hence, it is important to theoretically study critical conditions for their appearance and investigate their physical mechanism.

Naraghi *et al.* [60, 62] has suggested that there exists periodic distribution sites to accommodate local instabilities. It was also stated that the crack formation on the surface of nanofibres under stretching could facilitate the seeding of necks, which is analogous to the fragmentation of brittle films deposited on ductile substrates. By focusing on surface tension effects, Wu *et al.* [45] made the first attempt to interpret the evolution mechanism of surface rippling in polymeric nanofibres under axial stretching. For this purpose, a 1D phenomenological nonlinear elastic model has been developed to examine combined effects of surface tension and nonlinear elasticity on the formation of ripples. In this model, nanofibres are simplified as a homogeneous, isotropic and hyperelastic Mooney−Rivlin solid with a constant surface tension. The critical strain required to trigger surface rippling and the corresponding ripple wavelength were determined as a function of surface tension, elastic properties and fibre radius. The results indicated that the ripple wavelength increased with increasing fibre radius for a given set of elastic properties and surface tension of fibrous materials. However, the rate-dependent surface wrinkles cannot be explained by the study

conducted by Wu *et al.* [45] since it has been confirmed that polymeric fibres have cylindrical core–shell structures [42, 56].

Recent studies [63, 64] suggest that the difference of mechanical properties (e.g. mismatch of Young's moduli), rather than surface tension, play a dominant role in surface instabilities of core−shell structures and thin film/substrate structures. As a result, Tang *et al.* [61] adopted molecular dynamics (MD) and finite element (FE) simulations to investigate their hypotheses in which surface ripples of nanofibres were subjected to uniaxial tension owing to their core−shell microstructures. Based on MD and FE approaches, it was demonstrated that under tension different compressibilities between core and shell of polymeric layers could lead to surface wrinkling. It has also been stated that surface rippling of nanofibres is governed by a "polarisation" mechanism at the core−shell interphase regime that is ultimately induced by mismatches between Poisson's ratios or between Young's moduli as a secondary role. Further, by considering the plastic deformation in 3D FE calculations, the surface ripples can be tuned according to applied strain rate and yield strength of nanofibres.

Fibre diameter and structural morphology are the most important features of electrospun nanofibres that affect their performance in targeted functional applications as follows:

- *Biomedical Applications*: In the case of tissue-engineered substrates, it has been shown that the onset of fibroblast cell adhesion and migration depends on the minimum fibre diameter [65]. Moroni *et al.* [66] found that fibre diameters of electrospun polyethylene oxide terephthalate/polybutylene terephthalate (PEOT/PBT) scaffolds influenced cell seeding, attachment and proliferation. Cell response can also be affected by nanofibre diameter [67].
- *Filtration Applications*: Filtering applications are influenced by fibre size [68, 69] with filters manufactured from fibres. Smaller diameters generally possess higher filtration efficiency [70, 71].

- *Sensor Applications*: The sensitivity of sensors also increases with decreasing fibre diameter due to higher surface areas of fibres [72].
- *Composite Applications*: Electrospun nanofibres have been recognised as a good candidate material for reinforcement due to their high surface areas which are directly correlated with the toughness of composite materials. The surface area is intrinsically related to fibre diameter with any reduction in fibre diameter increasing the surface area to volume ratio [25, 73, 74]. Moreover, fibre diameter influences the transparency of resulting composites [75]. Hence the inter-relationship between fibre geometry, available surface area and pore dimensions in a fibrous network is crucial.
- *Other Applications*: Kim *et al.* [76] designed polymer batteries based on electrospun PVDF fibrous electrolyte. It is shown that lower mean fibre diameter results in a higher electrolyte uptake, thereby increasing the ionic conductivity of fibrous mats**.** Moreover, fibre size and morphology influence hydrophobic behaviour of polymers with Simsek *et al.* [77], which states that the water contact angle (hydrophobic surface) is affected by fibre size.

Consequently, numerous applications require well-tailored nanofibres with desired diameters and morphology, which suggests the importance for the precise control of these features. This aspect cannot be achieved without the comprehensive evaluation of quantitative studies on the effects of processing parameters during electrospinning. Despite the apparent simplicity of electrospinning principle, the process itself is relatively complicated due to the fact that many parameters influence fibre diameters and final morphological structures. These parameters can be classified into three main categories [78, 79]: (i) solution parameters (solution viscosity, concentration, molecular weight, surface tension, electrical conductivity, dipole moment, dielectric strength), (ii) processing parameters (feed rate, electric field strength, tip-to-collector distance, needle (tip) shape, collector type, composition and geometry) and (iii) ambient

parameters (temperature, relative humidity and air flow). Proper manipulation of these parameters is required in order to achieve desirable fibre morphology and diameter Several studies have addressed processing-property relationships in electrospun polymeric fibres and considered the key factors that determine electrospun fibre diameters with the results summarised in previous work [18, 23, 80, 81].

4. Models to Predict Electrospun Nanofibre Diameters

Many studies have been carried out in order to gain a deep understanding of electrospinning process for a better control of the fibre formation [82-84]. Due to the complexity and nonlinear relationships amongst parameters that affect nanofibre diameter, the determination of fibre diameters using a one factor-at-a-time approach is inefficient and time-consuming [85]. Furthermore, a qualitative description of experimental observations is inadequate to achieve consistent and generalised research outcomes. Despite great interests in different aspects of electrospinning processing, only a few studies have addressed the quantitative analysis of effects of processing parameters. In this respect, some empirical relationships have been suggested for the prediction of electrospun fibre morphology from a single fluid property. Detzil *et al.* [86] found a power law relationship between fibre diameter and polymer concentration; whereas Demir *et al.* [87] reported that fibre diameter is proportional to the cube of polymer concentration. It has also been shown that the radius jet of nanofibres is inversely related to the cube root of electrical conductivity of the solution [88]. Additionally, Hartman *et al.* [89] has demonstrated that the diameter of charged jet (D) was related to feed rate (Q) in the form of $D \sim Q^{0.048}$. Wang *et al.* [90, 91] have developed empirical scaling laws correlating operational parameters in electrospinning and molecular parameters to jet size and final fibre diameter. It has been shown that fibre diameter has an exponential relationship with solution viscosity using an exponent of 0.41. A dimensionless number known as the Berry number (Be) has been used to predict the diameter of electrospun fibres (d) with a power law equation ($d=\alpha$

$(Be)^{\beta}$) where α and β are experimental coefficients [92, 93]. McKee *et al.* [94, 95] demonstrated a uniform power-law relationship between polymeric fibre diameter and zero shear viscosity. Nonetheless, due to the lack of systematic and characterised experimentations with proper designs, the development of an empirical model has been inevitably impeded [96].

Several researchers have proposed analytical models for electrospinning based on the electrohydrodynamic theory for a slender body [97] to predict jet behaviour. Hohman *et al.* [32] employed a ‘‘whipping model’’ for the electrospinning process, which mathematically explains the interplay between the electric field and fluid properties to predict a “terminal” jet diameter. Models were also proposed to estimate the asymptotic behaviour of jet radius as a function of initial jet radius [98, 99]. From conventional continuum hydrodynamics, Fridrikh *et al.* [99] derived an expression for jet diameter, generated as a function of material properties such as solution conductivity, surface tension (γ), dielectric constant (ε), flow rate (Q), the current carried by the fibre (I) and the ratio of initial jet length to nozzle diameter (χ) as follows:

$$d = \left(\gamma\xi \frac{Q^2}{I^2} \frac{2}{\pi(2Ln(\chi-3))}\right)^{\frac{1}{3}} \quad (1)$$

Their predictions were in good agreement with experimental results for poly(ethylene oxide) (PEO) fibres as well as in a reasonable accordance with those for PAN fibres. The predicted accuracy of fibre diameter was found to depend on the charge carrying ability of the jet. The model may over-predict the stretching for poly(ε-caprolactone) (PCL) because it is a non-conducting polymer and the charge is mainly carried by the solvent. Another factor considered was the lack of volatility of solvents (*e.g.*, water and N,N-dimethyl formamide) that were used for electrospinning PAN and PEO, as opposed to highly volatile solvents (*e.g.*, methanol) used for electrospinning PCL. These differences between polymers and solvents were noted, but not explicitly expressed in the analytical model of Eq. (1). Nonetheless, the model provides a

simple analytical method to estimate fibre diameter with the reasonable agreement; whereas, Eq. (1) evaluates the terminal diameter by considering a stationary collector, and further fibre thinning can be obtained when using rotating collectors such as a rotating drum or a disk collector [100]. Thompson *et al.* [101] carried out a major study with an electrospinning model to investigate the effects of molecular and operational parameters on final electrospun fibre diameters. Many parameters were found to impact fibre diameter, amongst which five important parameters including volumetric charge density, tip-to-collector distance, initial jet radius, relaxation time, and solution viscosity have the most significant effect on jet radius. This study demonstrates the complexity of electrospinning process and the difficult implementation of model specifications to electrospun fibre systems. Following this, a correlation was developed by Helgeson and Wagner [102] to predict fibre diameter for electrospinning process using a dimensional analysis. They were successful to develop a correlation that could be used to predict the fibre diameter *a priori* by using the Ohnesorge number and developing a new dimensionless group. The predictions worked well for electrospinning parameters, resulting in smooth fibres, but deviated slightly for parameters where beading is known to occur. Although their correlation does not require the knowledge of zero shear viscosity, it needs the value of electrical conductivity that is much easier to measure than the viscosity. However, this empirical equation has one major limitation in that fibre diameters do not depend on fluid flow rate, which limits its application to laboratory scaled experiments with the assumption of a "steady state operation" rather than a manufacturing environment [27].

In summary, many models have been proposed that lay out a theoretical foundation for the development of a simple scaling analysis in order to relate fibre morphology to spinning solution properties and controllable processing parameters. However, these models have

conflicting requirements such as surface tension or solution viscosity, inclusion or exclusion of fluid flow rate or isotropic relations.

4.1 Response surface morphology (RSM)

Response surface methodology (RSM) is a combination of mathematical and statistical techniques. It is very useful for statistical modelling and analysis of problems in which a response of interest, affected by several variables, is aimed to be optimised [103]. Recently, studies have been carried out to determine the feasibility of RSM and to establish a quantitative relationship between electrospinning parameters and fibre diameters [104-106]. However, obtained results cannot be generalised for all polymer/solvent systems since they are highly dependent on polymer structure and chemistry [107].

Gu *et al.* [108] employed RSM for a quantitative study of polyacrylonitrile (PAN) nanofibres. Their standard deviations with mean values and standard deviations of fibre diameters as a function of polymer concentration can be acquired in the form of a quadratic equation. However, the limitation of this work was the use of a constant tip-to-collector distance, whose possible interaction with other parameters was not considered in their results. Yördem *et al.* [109] used RSM to correlate mean values and coefficient of variation (CV) of electrospun PAN nanofibres to solution concentration and applied voltage at three different spinning distances with a cubic polynomial used to fit the data. Consistent with the previous study [108], fibre diameter was found to be very sensitive to changes in solution concentration. Depending on the solution concentration and tip-to-collector distance levels, the applied voltage was also found to be a critical parameter, demonstrating the interactive effects of parameters. Such results appear to be contradictory to the observation of Gu *et al.* [108] that applied voltage played an insignificant role on resulting fibre diameters for a constant tip-to-collector distance. This disagreement is ascribed to the fact that the extent of the interaction of any two variables may depend on a third variable as demonstrated by Yördem *et al.* [109]. Karim *et al.* [110]

used RSM to evaluate the effects of supplied voltage, polymer concentration in solvent and flow rate not only on PAN fibre diameter but also on their mechanical properties and orientation (alignment). Sukigara *et al.* [111] reported experimental work via RSM to model mean fibre diameters of regenerated *Bombyx mori* silk using electrospinning by altering the electric field and solution concentration at two spinning distances. It was shown that the effect of applied voltage to create the electric field may be surprisingly small or conversely unexpectedly significant, depending on the solution concentration used for electrospinning of *Bombyx mori* silk. Their work set a good example to possible interactions between processing parameters that may also be expected for other polymers. In another work, the main effect and factorial interactions of two processing parameters, namely solution concentration and applied voltage on average fibre diameters and their standard deviations were studied [112]. The result is contradictory to those reported by Deitzel *et al.* [86] and Demir *et al.* [87], in which a power law relationship between fibre diameter and solution concentration was established with exponents of 0.5 and 3.0, respectively. The differences are ascribed to the splitting or splaying phenomena of electrospinning jet and various solution systems used.

4.2 Artificial Neural Networks (ANN)

Artificial neural networks (ANN) have been successfully implemented to modelling work for the control of electrospinning processes in recent years. ANN cannot create an equation similar to RSM. Instead, similar to a human brain, it estimates the response based on trained data in the enquired range [113]. In general, a neural network is an interconnected parallel structure, consisting of an input layer of neurons (independent variables), a number of hidden layers and an output layer (response). The goal of neural network modelling is to predict fibre diameters using a function of inputs, which are measured variables acting upon the output.

Sarkar and co-workers [27] employed artificial neural networks (ANNs) to predict fibre diameters for PEO nanofibres with solution concentration, electrical conductivity, flow rate

and electric field strength used as input variables to the model. Small standard deviations on all network predictions indicated the good consistency (*i.e.* low variation on the prediction performance of the network model). In another study [114], a nonlinear neural network model was used to analyse the dependence of fibre diameters on processing parameters and to simulate conditions for electrospinning nanofibres with diameters in the range of 40-60 nm. Based on a Pareto chart, it was found that flow rate is crucial to fibre diameter, which was followed by ambient room temperature (RT) and solution viscosity. This work suggests the effect of variables beyond conventional processing parameters for material formulation such as applied voltage, tip-to-collector distance and flow rate that have been previously reported in the literatures [32, 99] for controlling fibre diameter. In particular, it is indicated that temperature, relative humidity and surface tension are important parameters to reduce fibre diameter, among which the first two parameters have not been used previously in analytical models.

Khanlou *et al.* [115] employed both RSM and ANN to optimise and predict diameters of electrospun polymethyl methacrylate (PMMA) fibres. It was reported that ANNs surpassed RSM in terms of error percentage and correlation coefficient factor (i.e. R value). Nevertheless, in another study [113], the RSM model possessed much lower absolute percentage errors when compared to the ANN model (0.84 vs 1.60), which is indicative of better RSM performance.

Both RSM and ANN have been employed for different polymers to predict and optimise electrospun fibre diameters and their associated results, as summarised in detail in Table 1.

5. Porosity and Permeability Modelling of Electrospun Nanofibres

The small fibre diameter and porous structure of electrospun nanofibre mats give rise to a large specific surface area. The performance of nanoporous materials in applications such as adsorption, separation, filtering, catalysis, fluid storage and transport is determined by their

porous structure and connectivity. Nanoporous materials have to be optimised by controlling the size and distribution of porosity, corresponding to the requirements of particular applications [140-144]. Moreover, porosity can affect the mechanical properties of electrospun nanofibres with changes of porosity. For example, varying the porosity in the range from 75 to 92% leads to a significant change in yield strength from 0.457 to 1.886 MPa, which depends on nozzle diameter used to fabricate scaffolds [145]. Currently, the control of nanoporous size and porosity distributions in nanofibre mats is one of the key topics in nanotechnology.

Tehrani *et al.* [146] defined the web permeability index (WPI), which can properly describe the pore interconnectivity of fibrous scaffolds and quantify their architectural characteristics such as pore number, pore size, and scaffold porosity. An imaging analysis technique was employed to investigate WPI by modelling the formation of electrospun scaffolds with WPI values assigned to the response when electrospinning parameters were altered. Based on the response analysis, it was found that the most significant parameter is polymer concentration, which was followed by applied voltage, solution mixture and nozzle-to-collector distance. Kim *et al.* [147] used the Monte Carlo method to develop an algorithm for simulating the formation of imaginary multi-layered nanowebs. An estimation algorithm was developed using a ghost particle with zero volume and mass to estimate the pore size and distribution of various constructed nanowebs under different conditions. According to the dimensional analysis, penetration time is a function of fibre diameter, area ratio (defined as the ratio of the total area of a fibre occupying the web to the total collecting area) and number of layers. In addition, penetration time was found to be strongly dependent of pore size.

One of the most important parameters to affect nanofibre porosity is fibre-to-fibre contact. It is well documented that the pore structure of fibrous assembly can be predicted if the number of fibre contacts is known in the assembly [148-151]. Pan *et al.* [151], Sampson *et al.* [148,

149] and Komori and Makishima [152,153] have developed theories of fibre contacts for general fibre assembles with definite fibre aspect ratios similar to nonwoven materials.

The work conducted by Corte and Lloyd [154] was further extended by Sampson *et al.* [149,155] to incorporate the effect of fibre width. A new variable was introduced to characterise the fibrous network, known as mean coverage (*c*), which is defined as the expected number of fibres covering a point in the support plane of the network. The probability that a point in the plane of the network has a coverage, *c*, is given by Poisson probability as follows:

$$\boldsymbol{P(c)} = \frac{\boldsymbol{e^{-\bar{c}}\bar{c}^{c}}}{\boldsymbol{c!}} \qquad \text{c = 0, 1, 2,....} \tag{2}$$

Bagherzadeh *et al.* [156] modified this model and introduced a new theoretical analysis for multilayers of nanofibrous materials in order to obtain the number of fibre-fibre contacts. In this approach, initially the statistics of pore size for single-layered nanofibre mats was considered. Following this, equations were derived for 3D multilayer nanofibrous structures by superposing single-layer assembles. The average number of contacts per unit length in a multilayered nanofibrous mats ($N_{cont,\ \emptyset,\ fib}$) could be expressed in the following form:

$$\bar{N}_{\text{cont, } \emptyset, \text{ fib}} = (2n-1)\frac{4\pi \log(1/\varepsilon)}{\pi\omega + 8\omega A \log(1/\varepsilon)} \tag{3}$$

where ω is the mean fibre diameter, ε is the porosity, *t* is the multilayer mat thickness, *A* is fibre aspect ratio and *n* is the number of layers in multilayered mats. It has been found that increasing fibre diameters and network porosity significantly increases the number of fibre-to-fibre contacts within nano-/microfibrous structures. The mean pore radius $\bar{r}$ for a single-layered nanofibrous network is given by:

$$\bar{r} = \frac{\omega\sqrt{\pi}}{4}\left(\frac{1}{4\log(1/\varepsilon)}\right) + \frac{2A}{\pi} \quad (4)$$

It is shown that mean pore radius is a function of fibre diameter, network porosity and fibre aspect ratio. Compared with the existing theory [150], relatively good agreement with experimental results was obtained for predicting pore size distributions of nanofibre mats using this new theory [157]. A recent extension of Sampson model [158] allows for the estimation of individual pore dimensions. The model calculates an in-plane pore diameter based on fibre diameter (ω) and porosity (ε) with the return of an average pore height, depending on a shape factor for electrospun fibres. Assuming circular fibre cross-sections, in-plane pore diameter (d_{2D}) is twice pore height (h) as given by:

$$h = \frac{d_{2D}}{2} = -\frac{\omega}{\log(\varepsilon)} \quad (5)$$

Additionally, Sampson [158] showed that the specific surface area of a fibre mat is composed of fibres with various circular or rectangular geometries. These geometries are inversely associated with the shape factor of an individual fibre for the same given fibre perimeter. The upper shape factor limit is that of the circular fibre, which decreases as the cross-section flattens to a rectangular shape, leading to an increase in the specific surface area.

Since the pore size distribution and the pore length in fibrous media were found to be fractal-like and based on fractal theory and the capillary model, Shou *et al.* [159] developed an analytical model to quantify the effective diffusivity and its relation to the geometrical structure of nanofibrous media. Thereby, the dimensionless effective diffusivity is expressed in terms of fibre radius as follows:

$$\frac{D_{eff}}{D_b} = \frac{\varepsilon L_0^{D_\tau - 1}(2-D_f)\int_{\frac{D_f - 1}{D_f}\frac{\varepsilon}{1-\varepsilon}r}^{\frac{D_f - 1}{k D_f}\frac{\varepsilon}{1-\varepsilon}r} \frac{2R^{D_\tau + 1 - D_f}}{2R+3\lambda} dR}{(1-k^{2-D_f})(\frac{D_f - 1}{kD_f}\frac{\varepsilon}{1-\varepsilon}r)^{2-D_f}} \quad (6)$$

where k is the ratio between the maximum and minimum pore radii and ε is the porosity. D_τ, D_f and L_0 are tortuosity fractal dimension, fractal dimension of pore area and straight length of a channel, respectively. R and r are pore and fibre radii. λ is the mean free path of the gas molecules, as well as D_b and D_{eff} are bulk diffusivity and effective diffusion coefficient.

The proposed model was in good agreement with experimental data for both electrospun and conventional fibres. The influence of structural parameters on effective diffusivities of fibrous media was also investigated. By increasing porosity and fibre radius, an increase in dimensionless effective diffusivity was observed (Fig. 6a) [159].

One of the most important parameters for measuring the flow resistance or separation efficiency of species involved in such applications is permeability, which has been extensively studied over several decades [160-162]. In order to predict the through-plane permeability of randomly distributed electrospun nanofibre layers, a mechanistic model was developed [163]. In the case of electrospun nanofibres, due to their comparable radius to the mean free path of air molecules in this model, the slip velocity on the surface of nanofibres is considered, which is unlike the continuum hypothesis for gas flow passing coarse fibres. The fibrous system was represented as a series of cells of orthogonal fibres with random volumes. Through-plane permeability of fibrous layers *(k)* of fully random arrangement in terms of fibre volume fraction (c) and fibre radius (r) is presented by:

$$K = r^2 \frac{-0.6\ln(c) - 0.74 + c - 0.25c^2 + 2Kn[-0.6\ln(c) - 0.14 + 0.25c^2]}{4c(1+2Kn)} \quad (7)$$

where *Kn* is the Knudsen number. Good agreement between the predicted dimensionless permeability (k/r^2) and experimental data over a wide range of fibre volume fractions was obtained. For both nanofibres and microfibres, increasing the fibre volume fraction causes a decrease in permeability. A single dimensionless factor in terms of cell volume is proposed as a quantitative measure for the variation of randomness of fibre distribution. Interestingly, a linear increasing trend in dimensionless through-plane permeability was observed by increasing this factor (Fig. 6b). As a result, randomly distributed fibrous media are more permeable than ordered fibre arrays [163].

Although the high porosity and small inter-fibre distance of electropsun nanofibres provide high permeability, electrospun fibre mats demonstrate low compactive resistance, which may have an adverse effect on their hydraulic permeability efficiency at high pressure. Hence, it is important to investigate the amount of reduction in permeability upon compression for electrospun mats. It was reported [145] that under hydraulic flow, electrospun mats experienced a decrease of more than 60% in permeability between 5 and 140 kPa in that pressure-induced compression causes a loss of porosity, and thus membrane permeability decreases. To explain this behaviour, a model was used by combining three analytical models including Darcy's law for a compressible and porous medium, Happel's equation [164] to model the permeability of fibre mats, and Toll's equation [165] to investigate their compressibility. Permeance was shown to decrease with an increase in pressure drop, indicating that the solidities of electrospun mats increase as a result of compression under pressure driven flow, and that the rate of increase of the solidity depends on the compressibility.

6. Modelling MechanicalPproperties of Electrospun Nanofibre Mats

Electrospun nanofibres are mostly collected in the form of nonwoven mats for the purpose of reinforcements. Therefore, understanding the effect of processing parameters on mechanical

performance of electrospun nanofibre mats is crucial to control and design nonwoven fibrous mats to fulfil its targeted application for mechanical reinforcements.

Wu and Dzenis [166] considered the effect of surface energy on the mechanical performance of nanofibre mats. Adhesive contact was modelled in filaments as elastic contact between two elastic cylinders positioned at an arbitrary angle subjected to surface adhesion. It was assumed that filaments were uniform and smooth elastic cylinders. The equation that govern the adhesive contact in filaments is derived as:

$$P = \frac{4\pi\gamma R}{sin\varphi\alpha} \tag{8}$$

where P is the compressive force (*i.e.* resultant adhesive force between two filaments in contact), φ is the spatial angle between the filament-axes, γ is the fibre surface energy and R is the filament radius. The area of contact zone is calculated by using $A_c = \pi ab$ where a and b are defined as the elliptical semi-axes of the contact zone. Based on numerical results, the contact zone area decreases rapidly with increasing angle φ between two fibres due to the rapid decrease of adhesive force with growing angle φ between two filaments.

Further work [167] defined fibre collapse when a network of thin fibres underwent a small perturbation (*e.g.*, air flow, dust collision, *etc.*). Surrounding fibres in the network may deflect and stick to each other, further leading to nonlinear mechanical behaviour and even global collapse of the fibre network. To derive critical collapse distance between neighbouring fibre segments, a case of the collapse between two arbitrarily positioned nanofibres due to surface adhesion was considered. The fibres were assumed to possess the same fibre diameters, lengths and surface properties with the critical collapse distance, h_c, to induce fibre collapse as given by:

$$\frac{h_c}{r} = \frac{1}{24\sqrt{D}}\frac{\gamma}{Er}\left(\frac{L}{r}\right)^4 \quad (9)$$

where γ is the surface energy, E is Young's modulus of the fibre, r is fibre radius and L/r is the fibre aspect ratio. D is the determinant of a positive definite 2×2 matrix relating to fibre aspect ratio L/r, critical collapse distance, h_c, and angle between fibres θ. Numerical results demonstrate that for a fibre segment pair at a relatively large angle, the critical distance to induce the fibre collapse is independent of fibre radius with this distance associated solely with fibre aspect ratio and material intrinsic length (γ/E).

Stylianopoulos *et al.* [168] systematically investigated the influence of microstructural features of fibrous scaffolds on macroscopic mechanical properties. A multi-scaled computational model was used to simulate the mechanical response of electrospun polyurethane mats. It was found that tensile properties were sensitive to microstructural architecture. In the other work [169], the same model was applied to predict the mechanical behaviour of cellulose acetate. Fibre networks with varied degrees of alignment were generated with the simulations repeated to predict elastic moduli of resulting meshes. It was found that changes in fibre alignment may yield a 3.6-fold increase in elastic modulus for moderately aligned meshes and a 8.5-fold increase for highly aligned meshes. These results suggest that the overall mechanical response of meshes is mainly governed by properties of the microstructure (*i.e.* fibre alignment) [169].

To relate Young's modulus of eletrospun single fibres to their nonwoven fabrics and *vice versa*, Pai *et al.* [170] proposed two microstructure-based models for networks of nonwoven fibrous mats by assuming straight fibres and curved fibres. A four-fibre geometry was used to set up a representative volume element (RVE) model (Fig. 7).

The use of such a model with the assumption of straight fibres to calculate Young's modulus resulted in a value that fell below the experimental data; whereas, the model based on curved

fibres provided a quantitative relationship between Young's moduli of mats and those of the fibres themselves. The fibre curvature was observed to be a function of fibre diameter and it increased with decreasing fibre diameter. It has been detected that the porosity, intrinsic fibre modulus, fibre diameter, curvature and distance between junctions where fibres cross, make significant effects on Young's moduli of nonwoven fabrics [170].

To predict the tensile deformation behaviour of randomly-oriented electrospun nanofibre mats, a model was developed by Wei *et al.* [171] using a MD simulation. In this model, nanofibres were represented by a chain of beads where each bead was a small segment of nanofibres. More specifically, beads were held together by bond interactions while beads and bonds were considered as joints and rods, respectively. Due to solvent evaporation during the electrospinning process, the inter-fibre contact could lead to fibre fusion. Such fibre-fibre fusion was assumed to be a chemical bond and the fusions were randomly distributed in nanofibre mats. Therefore, interactions between nanofibres were described by bonded (stretching, bending and torsion) and non-bonded (van der Waals interactions) potentials. A nanofibre network was generated into a square sample, consisting of several hundred randomly oriented filaments. Fibre-fibre fusion points were introduced randomly to evaluate the effect of various levels of fusion on mechanical properties of fibrous networks/mats. In case of no fusion in the nanofibre network, Young's modulus and tensile strength were half of those with fused networks (either in full or half fusions). Interestingly, both full and half fusions exhibited little difference in Young's modulus and tensile strength (Fig.8a). The introduction of fusion points significantly enhances the load transfer between fibres, thus enhancing the tensile strength. Fracture energy in nanofibres initially increases and then decreases with increasing normalised fusion; whereas, the strength at failure increases continuously with an increase in fusion (Fig. 8b). It has been shown that fibre-fibre fusion has a significant effect on tensile

properties of electrospun mats. Increasing the fibre-fibre fusion point enhances the tensile strength. However, it may lead to a decrease in fracture energy if over fusion occurs [171].

Rizvi *et al.* [172] used a mathematical model to analyse the influence of fibre assembly on macroscopic mechanical properties of fibrous materials. The model describes microstructural properties of a fibrous matrix using a probability density function. Three groups of fibres were assumed in the model, namely curved non-load-bearing fibres, straight load-bearing fibres and broken non-load-bearing fibres. Based on simulation results, more flexible fibres did not make fibrous matrices more flexible but instead led to higher load-bearing capacity of fibrous matrices (Fig. 9a). In case of the variation of fibre diameters, since the cross-sectional area of a fibre is a quadratic function of fibre diameter, an increase in fibre diameter resulted in a quadratic increase in strength of fibre matrices without changing the yield strain or strain at failure (Fig. 9b).

Moreover, it was indicated that when shorter and straighter fibres were used in matrices while maintaining the population of curved fibres, the yield strain of matrices was reduced but their strain at failure remained unchanged. In contrast to this, when longer and more curved fibres were introduced into matrices, the opposite effect was evident. Thus it is clear that fibre alignment plays a crucial role in mechanical properties of fibrous matrices. Randomly distributed fibres in a matrix demonstrate higher flexibility at the cost of lower load-bearing capacity and vice versa. Overall, to obtain a specific type of mechanical behaviour in a fibrous material, existing materials can be employed by selecting an appropriate structure in order to achieve desirable mechanical properties rather than using a new fabricated material [172].

To gain insight into the mechanical behaviour of fibrous matrices under a large amount of elongation as well as shear, a statistical model has been recently formulated [173]. The influence of structural parameters (*i.e.* fibre curvature, orientation and alignment) on the mechanical response of the matrix was investigated with the load–deformation relationships

for fibrous matrices with different structural parameters determined. It has been demonstrated that the density of load bearing fibres is not homogeneous within fibrous matrices. Additionally, the mechanical response of fibrous matrices was also found to be dependent on the aspect ratio of matrices. In particular, fibre tension inside the matrices can be reduced with increasing aspect ratio under both shear and elongation deformations and its effect is more significant for the latter. In the other work [174], a finite element model was employed to determine the effect of fibre aspect ratio and orientation on shear strain distribution within electrospun nanofibrous assemblies. Main results has shown that samples with a lower aspect ratio cause more uniform distribution of shear strain.

Gomez-Pachon *et al.* [175] developed mathematical models using a homogenisation and differential replacement method (DRM) to predict effective Young's modulus of semicrystalline PLA nanofibre scaffolds in view of their internal morphology with the consideration of two PLA phases (*i.e.* amorphous and lamellar phases). One is referred to as a laminate bimaterial periodic structure (LBPS), and the other as a hierarchical bimaterial cylindrical structure (HBCS) (Fig. 10). The latter is based on a theory that the internal nanofibrous structure is most likely to be hierarchically composed of two parts, namely an internal core and an external shell. The predicted data based on both models were in good agreement with corresponding experimental results. Furthermore, it was shown that with the addition of supramolecular layers around the amorphous core of PLA electrospun nanofibres, Young's modulus increased in a monotonic manner.

As electrospun nonwoven materials exhibit a particularly high number of fibre-fibre junctions, interfibre interaction is particularly important in determining macroscopic mechanical properties of such mats. It is shown that thermal treatment [176] or residual solvents [177,178] in electrospun fibres can yield interfibre bonding and improved mechanical properties. Buell *et al.* [179] performed detailed MD simulations at an atomistic level for

electrospun nanofibres to explore a very short range of fibre interactions. It is noteworthy that MD simulations demonstrate a considerable force of attraction for nanofibres that are aligned in the parallel direction at a distance of 9 nm; whereas, based on a molecular statics approach, a transition from an attractive force to a repulsive force at a separation distance of 6 nm was predicted. This discrepancy can be explained in terms of extent differences of molecular mobility within and between fibres for these various modelling perspectives.

It is also possible to investigate the effect of electrospinning processing on the mechanical behaviour of nanofibres by employing a neural network model. Vatankhah *et al.* [180] evaluated the simultaneous effects of composition, fibre diameter and fibre orientation of electrospun PCL/gelatin mats on elastic moduli of scaffolds by using a neural network model. The elastic modulus was determined in both circumferential (*i.e.* the direction of mandrel rotation) and longitudinal (*i.e.* perpendicular to the direction of mandrel rotation) directions for fibres with different alignment indices. It is evident that aligned nanofibrous mats show anisotropic mechanical behaviour, which is consistent with their architectural anisotropy. Moreover, depending on the composition, fibre diameter and orientation, as well as elastic moduli in the range of 1.0–140 MPa can be obtained under ambient conditions.

7. Conclusions

Several novel models and optimisation methods have been discussed to be correlated with experimental observations of electrospun nanofibres. These include diameter, porosity, permeability, size effect in mechanical properties, wave propagation, surface rippling and mechanical properties. Despite the relatively early introduction of electrospinning process, the control of morphology and mechanical behaviour of nanofibres is still under significant investigation. The lack of understanding and absence of a theoretical framework to predict these features may ultimately prevent electrospun nanofibres from their applications to full potential regardless of other merits. There is much knowledge to be gained in further modelling

routes, especially with regards to the evolution of nanoscaled structures and the control of parameters. These models are deemed useful to provide a novel and fundamental understanding of principles for the manufacture and characterisation of continuous electrospun nanofibres for widespread applications.

References

1. Shabafroozi, V.; Mozafaril, M.; Vashaee, D.; Tayebil, L. *J. Nanosci. Nanotechnol.* **2014**, 14, 522.
2. Fang, J.; Wang, X.; Lin, T. *Nanofibers - Production, Properties and Functional Applications*; InTech: Croatia, **2011**; Chapter 14, pp. 287-326.
3. Lu, P.; Ding, B. *Recent Pat. Nanotechnol*. **2008**, 2, 169.
4. Sun, T.; Norton, D.; Ryan, A. J. MacNeil, S.; Haycock, J. W. *J. Mater. Sci. Mater. Med.* **2007**,18, 321.
5. Ekaputra, A. K.; Prestwich, G. D.; Cool, S. M.; Hutmacher, D. W. *Biomacromolecules*. **2008**, 9, 2097.
6. Pham, Q.P.; Sharma, U.; Mikos, A. G. *Biomacromolecules* **2006**, 7, 2796.
7. Burman, M.; Arinstein, A.; Zussman, E. *Appl. Phys. Lett.* **2008**, 93, 193118.
8. Arinstein, A.; Burman, M.; Gendelman, O.; Zussman, E. *Nat. Nanotechnol*. **2007**, 2, 59.
9. Atwood, R. C.; Jones, J. R.; Lee, P. D.; Hench, L. L. *Scr. Mater*. **2004**, 51, 1029.
10. Engler, A. J.; Sen, S.; Sweeney, H. L.; Discher, D. E. (2006) *Cell*. **2006**,126, 677.
11. Rao, N.; Grover, G. N.; Vincent, L. G.; Evans, S. C.; Choi, Y. S.; Spencer, K. H.; Hui, E. E.; Englerac, A. J.; Christman, K. L. *Integr. Biol*. **2013**, 5, 1344.
12. Ellison, C. J.; Phatak, A.; Giles. D. W.; Macosko, C. W.; Bates, F. S. *Polymer* **2007**, 48, 3306.
13. Li, H.; Ke, Y.; Hu, Y. *J. Appl. Polym. Sci.* **2006**, 99, 1018.
14. Ma, P. X.; Zhang, R. *J. Biomed. Mater. Res.* **1999**, 46, 60.

15. Yanga, Z.; Xu, B. *J. Mater. Chem.* **2007**, 17, 2385.

16. Reneker, D. H.; Doshi, J. *Nanotechnology*. **1996**, 7, 216.

17. Dzenis, Y. *Science* **2004**, 304, 1917.

18. Reneker, D. H.; Yarin, A. L.; Zussman, E.; Xu, H. *Adv. Appl. Mech.* **2007,** 41, 43.

19. Reneke,r D.H. Yarin, A. L. *Polymer* **2008,** 49, 2387.

20. Cooley, J. F. US Patent, 692631, **1902**.

21. Morton, W. J. US Patent, 705691**, 1902**.

22. Formhals A (1934) Process and apparatus for preparing artificial threads. US1975504 A

23. Huang, Z. M.; Zhang, Y. Z.; Kotaki, M.; Ramakrishna, S. *Compos. Sci. Technol.* **2003**, 63, 2223.

24. Bhardwaj, N.; Kundu, S. C. *Biotechno.l Adv.* **2010**, 28, 325.

25. Mohammadzadehmoghadam, S.; Dong, Y.; Davies, I. J. *J. Polym. Sci. Pt B-Polym. Phys.* **2015,** 53, 1171.

26. Baji, A.; Mai, Y. W.; Wong, S. C.; Abtahi, M.; Chen, P. *Compos. Sci. Technol.* **2010,** 70, 703.

27. Sarkara, K.; Ghaliab, M. B.; Wu Z, Bose, S. C. *J. Mater. Process. Technol*. **2009,** 209, 3156.

28. Ye, X. Y.; Lin, F. W.; Huang, X. J.; Liang, H. Q.; Xu, Z. K. *RSC. Adv.* **2013**, 3, 13851.

29. Yarin, A. L.; Koombhongse, S.; Reneker, D. H. *J. Appl. Phys.* ***2001***, 90, 4836.

30. Spivak, A. F.; Dzenis, Y. A.; Reneker, D. H. *Mech. Res. Commun.* **2000,** 27, 37.

31. Feng, J. J. *J. Non-Newton. Fluid. Mec.h* **2003**, 116, 55.

32. Hohman, M. M.; Shin, M.; Rutledge, G.; Brenner, M. P. *Phys. Fluids* **2001**, 13, 2201.

33. Wu, X. F.; Salkovskiy, Y.; Dzenis, Y. A. *Appl. Phys. Lett*. **2011**, 98, 223108.

34. Taylor, G. I. *Proc. R. Soc. London. Ser A. Math. Phys. Sci.* **1964**, 280, 383.

35. Taylor, G. I. *Proc. R. Soc. London. Ser A. Math. Phys. Sci*. **1966**, 291, 159.

36. Pisignano, D. *Polymer Nanofibers: Building Blocks for Nanotechnology*; RSC Publishing: Cambridge, **2013**; Chapter 2, pp. 50-131.

37. Refiei, S.; Maghsoodloo, S.; Noroozi, B.; Mottaghitalab, V.; Haghi, A. K. *Cellulose. Chem. Technol.* **2013**, 47, 323.

38. Pai, C. L.; Boyce, M. C.; Rutledge, G. C. *Polymer* **2011**, 52, 2295.

39. Croisier, F.; Duwez, A. S.; Jérôme, C,; Léonard, A. F.; van der Werf, K. O.; Dijkstra, P. J.; Bennink, M. L.; *Acta. Biomater*. **2012,** 8, 218.

40. Zussman, E.; Burman, M.; Yarin, A. L.; Khalfin, R.; Cohen, Y. *J. Polym. Sci. Pt B-Polym. Phys.* **2006**, 44, 1482.

41. Carlisle, C. R.; Coulais, C.; Guthold, M. *Acta. Biomater*. **2010**, 6, 2997.

42. Naraghi, M.; Arshad, S. N.; Chasiotis, I. *Polymer* **2011**, 52, 1612.

43. Shin, M. K.; Kim, S. I.; Kim. S. J.; Kim, S. K.; Lee, H.; Spinks, G. M. *Appl. Phys. Lett.* **2006**, 89, 231929.

44. Wong, S. C.; Baji, A.; Leng, S. *Polymer* **2008**, 49, 4713.

45. Wu, X. F.; Kostogorova-Beller, Y. Y.; Goponenko, A. V.; Hou, H.; Dzenis, Y. A. *Phys. Rev. E.* **2008**, 78, 061804.

46. Wu, X. F.; Dzenis, Y. A. *J. Appl. Phys.* **2007**, 102, 044306.

47. Dingreville, R.; Qu, J.; Cherkaoui, M. *J. Mech. Phys. Solids.* ***2005***, 53, 1827.

48. Cuenot, S.; Fretigny, C.; Demoustier-Champagne, S.; Nysten, B. *Phys. Rev. B.* **2004**, 69, 65410.

49. Hwang, K. Y.; Kim, S. D.; Kim, Y. W.; Yu, W. R. *Polym. test.* **2010**, 29, 375.

50. Lim, C. T.; Tan, EPS; Ng, S. Y.; *Appl. Phys. Lett.* **2008**, 92,141908.

51. Stachewicz, U.; Bailey, R. J.; Wang, W.; Barber, A. H.; *Polymer* **2012**, 53, 5132.

52. Papkov, D.; Zou, Y.; Andalib, M. N.; Goponenko, A.; Cheng, SZD.; Dzenis, Y. A. *ACS. Nano.* **2013**, 7, 3324.

53. Ji, Y.; Li, C.; Wang, G.; Koo, J.; Ge, S.; Li, B.; Jiang, J.; Herzberg, B.; Klein, T.; Chen, S,.; Sokolov, J. C.; Rafailovich, M. H. *Europhys let.* **2008**, 84, 56002.

54. Baji, A.; Mai, Y. W.; Wong, S. C. *Polym. Eng. Sci.* **2014**, 55, 1812.

55. Curgul, S.; Van Vliet, K. J.; Rutledge, G. C. *Macromolecules* **2007**, 40, 8483.

56. Camposeo, A.; Greenfeld, I.; Tantussi, F.; Pagliara, S.; Moffa, M.; Fuso, F.; Allegrini, M.; Zussman, E.; Pisignano, D. *Nano. Let.* **2013**, 13, 5056.

57. Arinstein, A. *J. Polym. Sci. Pt B-Polym. Phys.* **2013**, 51, 756.

58. Tang, S.; Greene, M. S.; Liu, W. K. *Appl. Phys. Lett.* **2011**, 99, 191910.

59. Yuan, B.; Wang, J.; Han, RPS. *J. Mech. Behav. Biomed. Mater.* **2015,** 42, 26.

60. Naraghi, M.; Chasiotis, I.; Kahn, H.; Wen, Y. K.; Dzenis, Y. *Appl. Phys. Lett.* **2007**, 91, 151901.

61. Tang, S.; Li, Y.; Liu, W. K.; Huang, X. X. *Macromolecules* 2014, 47, 6503.

62. Naraghi, M.; Chasiotis, I.; Kahn, H.; Wen, Y.; Dzenis, Y. *Rev. Sci. Instrum.* ***2007,*** 78, 085108.

63. Li, B.; Jia, F.; Cao, Y. P.; Feng, X. Q.; Gao, H. (2011) *Phys. Rev. Lett.* **2011**, 106, 234301.

64. Li, B.; Cao, Y. P.; Feng, X. Q.; Gao, H. *Soft Matter* **2012**, 8, 5728.

65. Sun, T.; Norton, D.; Ryan, A. J.; MacNeil, S.; Haycock, J. W. *J. Mater. Sci. Mater. Med.* **2007**, 18, 321.

66. Moroni, L.; Licht, R.; de Boer, J.; de Wijn, J. R.; van Blitterswijk, C. A. *Biomaterials*, **2006**, 27,4911.

67. Pelipenko, J.; Kocbek, P.; Kristl, J. *Eur. J .Pharm. Sci.* **2014**, 66, 29.

68. Shin, C.; Chase, G. G.; Reneker, D. H. *Colloid. Surf. A-Physicochem. Eng. Asp.* **2005**, 262, 211.

69. Grafe, T. H.; Graham, K. M. *Nanofiber webs from electrospinning*, Proceeding of 5th International Conference on Nonwovens in Filtration; Germany, **2003**; pp. 1-5.

70. Podgóski, A.; Bałazy, A.; Gradoń, L. *Chem. Eng. Sci*. **2006**, 61, 6804.

71. Qin, X. H.; Wang, S. Y. *J. Appl. Polym. Sci*. **2006,** 102, 1285.

72. Ding, B.; Yamazaki, M.; Shiratori, S. (2007) *Sens. Actuator. B-Chem.* **2007**, 106, 477.

73. Neppalli, R.; Causin, V.; Marigo, A.; Meincken, M.; Hartmann, P.; van Reenen, A. J. *Polymer* **2013**, 54, 5909.

74. Tang, C.; Wu, M.; Wu, Y.; Liu, H. *Compos. Part. A-Appl. S.* **2011**, 42, 1100.

75. Bergshoef, M. M.; Vancso, G. J. (1999) *Adv .Mater.* ***1999***, 11, 1362.

76. Kim, J. R.; Choi, S. W.; Jo, S. M.; Lee, W.S.; Kim, B. C. *Electrochim Acta* **2004**, 50, 69.

77. Acatay, K.; Simsek, E.; Ow-Yang, C.; Menceloglu, Y. Z. *Angew. Chem. Int. Ed.* **2004,** 43, 5210.

78. Rogina, A. *Appl. Surf. Sci*.**2014**, 296, 221.

79. Ingavle, G. C.; Leach, J. K. *Tissue Eng. Part. B. Rev*. **2014**, 20, 277.

80. Khan, W. S.; Asmatulu, R.; Ceylan, M.; Jabbarnia, A. *Fiber. Polym.* **2013**, 14, 1235.

81. Wendorff, J. H.; Agarwal, S.; Greiner, A. Electrospinning: Materials, Processing and Applications; Wiley-VCH: Weinheim, **2012**; Chapter 3, pp. 69-104.

82. Casper, C. L.; Stephens, J. S.; Tassi, N. G.; Chase, D. B.; Rabolt, J. F. *Macromolecules* **2004**, 37,573.

83. Zhang, D.; Chang, J. *Nano. Lett.* **2008**, 8, 3283.

84. Yee, W. A.; Kotaki, M. Liu, Y.; Lu, X. *Polymer* **2007**, 48,512.

85. Sarkar, K.; Ghalia, M. B.; Wu, Z.; Bose, S. C.; Sarkar, K.; Ghalia, M. B.; Wu, Z.; Bose, S. C. *J. Mater. Process. Techno.l* **2009**, 209, 3156.

86. Deitzel, J. M.; Kleinmeyer, J.; Harris, D.; Tan, NCB. *Polymer* **2001**, 42, 261.

87. Demir, M. M.; Yilgor, I.; Yilgor, E.; Erman, B. *Polymer* **2002**, 43, 3303.

88. Huang, L.; Nagapudi, K.; Apkarian, P. R.; Chaikof, E. L. *J. Biomater. Sci. Polym. Ed.* **2001**, 12,979.

89. Hartman, R.; Brunner, D.; Camelot, D.; Marijnissen, J.; Scarlett, B. *J. Aerosol. Sci.* **2000**, 31, 65.

90. Wang, C.; Hsu, CH.; Lin, J. H. *Macromolecules* **2006**, 39, 7662.

91. Wang, C.; Hsu, C. H.; Hwang, I. H. *Polymer* **2008**, 49, 4188.

92. Cengiz, F.; Krucińska, I.; Glisć, ińska. E. *Fibers. Text East. Eur.* **2009**, 17, 13.

93. Erencia, M.; Cano, F.; Tornero, J. A.; Macanás, J.; Carrillo, F. *Langmuir* **2014**, 30, 7198.

94. McKee, M. G.; Layman, J. M.; Cashion, M. P.; Long, T. E. *Science* **2006**, 311, 353.

95. McKee, M. G.; Wilkes, G. L.; Colby, R. H.; Long, T. E. *Macromolecules* **2004**, 37,1760.

96. Ziabari, M.; Mottaghitalab, V.; Khodaparast Haghi, A. *Korean. J. Chem. Eng.* **2010**, 27, 340.

97. Saville, D. A. *Ann. Rev. Fluid. Mech.* **1997**, 29, 27.

98. Feng, J. J. *J. Non-Newtonian. Fluid. Mech.* ***2003***, 116, 55.

99. Fridrikh, S. V.; Yu, J. H.; Brenner, M. P.; Rutledge, G. C. *Phys. Rev. Lett.* **2003**, 90, 144502.

100. Yee, W. A.; Nguyen, A. G.; Lee, P. S.; Kotaki, M.; Liu, Y.; Tan, B. T. *Polymer* **2008**, 49, 4196.

101. Thompson, C. J.; Chase, G. G.; Yarin, A. L.; Reneker, D. H. *Polymer* **2007**, 48, 6913.

102. Helgeson, M. E.; Wagner, N. J. *Amer. Inst. Chem. J.* **2007**, 53, 51.

103. Gonen, S. O.; Taygun, M. E.; Kuçukbayrak, S. *Chem. Eng. Technol.* **2015**, 38, 844.

104. Ray, S.; Lalman, J. A. *Chem. Eng. J.* **2011**, 169, 116.

105. Padmanabhan, T.; Kamaraj, V.; Magwood Jr, L.; Starly, B. *J. Manuf. Processes.* **2011**, 13,104.

106. Neo, Y. P.; Ray, S.; Easteal, A. J.; Nikolaidis, M. G.; Quek, S. Y. *J. Food. Eng.* **2012**, 109, 645.

107. Roso, M.; Lorenzetti, A.; Besco, S.; Monti, M.; Berti, G.; Modesti, M. *Comput. Chem. Eng.* **2011**, 35, 2248.

108. Gu, S. Y.; Ren, J.; Vancso G. J. *Eur. Polym. J.* **2005**, 41, 2559.

109. Yordem, O. S.; Papila, M.; Menceloglu, Y. Z. *Mater. Des.* **2008**, 29, 34.

110. Karim, S. A.; Sulong, A. B.; Azhari, C. H.; Lee, T. H.; Hwei, N. M. *J. Appl. Sci. Res.* **2012**, 8, 2510.

111. Sukigara, S.; MGandhi, M.; Ayutsede, J.; Micklus, M.; Ko, F. *Polymer* **2004**, 45, 3701.

112. Gu, S. Y.; Ren, J. *Macromol. Mater. Eng*. **2005**, 290, 1097.

113. Nasouri, K,; Bahrambeygi, H.; Rabbi, A.; Mousavi Shoushtari, A.; Kaflou, A. *J. Appl. Polym. Sci. **2012***, 126,127.

114. Costolo, M. A.; Lennhoff, J. D.; Pawle, R.; Rietman, E. A.; Stevens, A. E. *Nanotechnology* 2**008**, 19, 035707.

115. Mohammad Khanlou, H.; Sadollah, A.; Ang, B. C.; Kim, J. H.; Talebian, S.; Ghadimi, A. *Neural Comput Appl* **2014**, 25,767.

116. Ahmadipourroudposht, M.; Fallahiarezoudar, E.; Mohd Yusof, N.; Idris, A. *Mater. Sci. Eng. C.* **2015**, 50, 234.

117. Ali, A. A.; Eltabey, M. M.; Farouk, W. M.; Zoalfakar, S. H. *J. Electrost.* **2014**, 72, 462.

118. Maleki, H.; Gharehaghaji, A. A.; Criscenti, G.; Moroni, L.; Dijkstra, P. J. *J. Appl. Polym. Sci*. **2015**, 132, 41388.

119. Jia, O.; Jiao, X.; Li, S. *Adv. Mater. Res*. 332–334, 1318.

120. Park, J. Y.; Shim, W. G.; Lee, I. H. *J. Nanosci. Nanotechnol.* **2011**, 11, 1359.

121. Naghibzadeh, M.; Adabi, M. *Fiber. Polym.* **2014**, 15, 767.

122. Pezeshki-Modaress, M.; Zandi, M. Mirzadeh, H. *Polym. Int.* **2015**, 64,571.

123. Pezeshki-Modaress, M.; Mirzadeh, H.; Zandi, M. *Mater. Sci. Eng.* C. **2015**, 48, 704.

124. Askari, M.; Rezaei, B.; Mousavi Shoushtari, A.; Noorpanah, P.; Abdouss, M.; Ghani, M. *Can. J. Chem. Eng.* **2014**, 92, 1008.

125. Gholipour, A.; Bahrami, S. H.; Nouri, M. *e-Polym.* **2010**, 10, 361.

126. Aliabadi, M.; Irani, M.; Ismaeili, J.; Najafzadeh, S. *J. Taiwan. Inst. Chem. Eng.* **2014**, 45,518.

127. Agarwal, P.; Mishra, P. K.; Srivastava, P. *J. Mater. Sci*. **2012**, 47, 4262.

128. Konwarh, R.; Misra, M.; Mohanty, A. K.; Karak, N. *Carbohydr. Polym.* **2013**, 92, 1100.

129. Jacobs, V.; Patanaik, A.; Rajesh, D.; Maaza, A. M. *Curr. Nanosci.* **2011**, 7, 396.

130. Amiraliyan, N.; Nouri, M.; Haghighat Kish, M.; *Fiber. Polym.* **2009**, 10, 167.

131. Chen, J. P.; Ho, K. H.; Chiang, Y. P.; Wu. K. W.; *J. Membr. Sci.* **2009**, 340, 9.

132. Tsimpliaraki, A.; Zuburtikudis, I.; Imarras, S.; Panayiotou, C. *Polym. Int.* **2011**, 6, 859.

133. Tsimpliaraki, A.; Svinterikos, S.; Zuburtikudis, I.; Marras, S. I.; Panayiotou, C. *Ind. Eng. Chem. Res.* **2009**, 48, 4365.

134. Sarlak, N.; Farahmand Nejad, M. A.; Shakhesi, S.; Shabani, K. *Chem. Eng. J.* **2012**, 210, 410.

135. Naderi, N.; Agend, F.; Faridi-Majidi, R.; Sharifi-Sanjan, N.; Madani, M.; *J. Nanosci. Nanotechnol.* **2008**, 8, 2509.

136. Kong, L.; Ziegler, G. R. *Carbohydr. Polym.* **2013**, 92, 1416.

137. Mirzaei, E.; Amani, A.; Sarkar, S.; Saber, R.; Mohammadyani, D.; Faridi-Majidi, R. J *Appl. Polym. Sci.* **2012**, 125, 1910.

138. Rabbi, A.; Nasouri, K.; Bahrambeygi, H.; Mousavi Shoushtari, A.; Babaei, M. R. *Fiber. Polym.* **2012**, 13, 1007.

139. Faridi-Majidi, R.; Ziyadi, H.; Naderi, N.; Amani, A. *J. Appl. Polym. Sci.* **2012**, 124, 1589.

140. Xu, L.; Wu, Y.; Nawaz, Y. *Comput. Math. Appl.* **2011**, 61, 2116.

141. Harel, E.; Granwehr, J.; Seeley, J. A.; Pines, A. *Nat. Mater.* **2006**, 5, 321.

142. Alomari, A. K. *Comput. Math. Appl.* **2011**, 61, 2528.

143. Aksoy, Y.; Pakdemirli, M. *Comput. Math. Appl.* **2010**, 59, 2802.

144. Xua, L.; Liu, F.; Faraz, N. *Comput. Math. Appl.* **2012**, 64, 1017.

145. Choong, L. T.S.; Khan, Z.; Rutledge, G. C. *J. Membr. Sci.* **2014**, 451, 111.

146. Heidarkhan Tehrani, A.; Zadhoush, A.; Karbasi, S.; Nouri Khorasani, S. *J. Appl. Polym. Sci.* **2010**, 118, 2682.

147. Kim, H.; Kim, D. W.; Seo, M. H.; *Macromol. Res.* **2005**, 13, 107.

148. Sampson, W. W. *J. Mater. Sci.* **2001**, 36, 5131.

149. Sampson, W. W. *J. Mater. Sci.* **2003**, 38, 1617.

150. Eichhorn, S. J.; Sampson, W. W. *J. Royal. Soc. Interf.* **2005**, 2, 309.

151. Pan, N.; He, J. H.; Yu, J. *Text. Res. J.* **2007**, 77,205.

152. Komori, T.; Itoh, M. *Tex Res. J.* **1994**, 64, 519.

153. Komori, T.; Makishima, K. *Text. Res. J.* **1977**, 47, 13.

154. Corte, H. K.; Lloyd, E. H. *Consolidation of the Paper Web*; British Paper and Board Makers' Association: London, **1966**; Vol. 2, pp. 981-1009.

155. Sampson, W. W. *J. Mater. Sci.* **2004**, 39, 2775.

156.Bagherzadeh, R.; Shaikhzadeh Najar, S.; Latifi, M.; Tehran, M. A.; Kong, L. *J. Biomed. Mater. Res. Part A.* **2013,** 101A, 2107.

157.Bagherzadeh, R.; Latifi, M.; Shaikhzadeh Najar, S.; Kong, L. *J. Ind. Text.* **2014**, 43, 483.

158. Eichhorn, S. J.; Sampson, W. W. *J. R. Soc. Interface*. **2010,** 7, 641.

159. Shou, D.; Fan, J.; Mei, M.; Ding, F. *Microfluid. Nanofluid.* **2014,** 16, 381.

160. Gebart, B. R. *J. Compos. Mater.* **1992**, 26, 1100.

161. Tamayol, A.; Bahrami, M. *Int. J. Heat. Mass. Transf.* **2009,** 52, 2407.

162.Brown, R. C. *Air Filtration: An integrated approach to the theory and application of fibrous filters*; Pergamon Press: New York, **1993**.

163. Shou, D.; Ye, L.; Fan, J. *Polymer* **2014**, 55, 3149.

164. Happel, J. *AIChE. J.* **1959**, 5174.

165. Toll, S. *Polym. Eng. Sci.* **1998**, 38, 1337.

166. Wu, X. F.; Dzenis, Y. A. *J. Phys. D-Appl. Phys.* **2007**, 40, 4276.

167. Wu, X. F.; Dzenis, Y. A. *Nanotechnology* **2007,** 18, 285702.

168. Stylianopoulos, T.; Bashur, C. A.; Goldstein, A. S.; Guelcher, S. A.; Barocas, V. H. *J. Mech. Behav. Biomed. Mater.* **2008**, 1, 326.

169. Stylianopoulos, T.; Kokonou, M.; Michael, S.; Tryfonos, A.; Rebholz, C.; Odysseos, A. D.; Doumanidis, C. *J. Biomed. Mater. Res. Part B.* **2012**, 100B, 2222.

170. Pai, C. L.; Boyce, M. C.; Rutledge, G. C. *Polymer* **2011**, 52, 6126.

171. Wei, X.; Xia, Z.; Wong, S. C.; Baji, A. *Int. J. Exp. Comput. Biomech.* **2009**, 1, 45.

172. Rizvi, M. S.; Kumar, P.; Katti, D. S.; Pal, A. *Acta. Biomater.* **2012**, 8, 4111.

173. Rizvi, M. S.; Pal, A. *J. Mech. Behav. Biomed. Mater.* **2014**, 37, 235.

174. Driscoll, T. P.; Nerurkar, N. L.; Jacobs, N. T.; Elliott, D. M.; Mauck, R. L.; *Mech. Behav. Biomed. Mater.* **2001**, 4, 1627.

175. Gomez-Pachon, E. Y.; Sanchez-Arevalo, F. M.; Sabina, F. J.; Maciel-Cerda, A.; Campos, R. M.; Batina, N.; Morales-Reyes, I.; Vera-Graziano, R. *J. Mater. Sci.* **2013**, 48, 8308.

176. Choi, S.; Lee, S. G.; Joo, C. W.; Im, S. S.; Kim, S. H. *J. Mater. Sci.* **2004**, 39, 1511.

177. Krishnapp,a R. V. N.; Desai, K.; Sung, C. J. *J. Mater. Sci.* **2003**, 38, 2357.

178. Kidoaki, S.; Kwon, K.; Matsuda, T. *J. Biomed. Mater. Res. Part. B.* **2006**, 76B, 219.

179. Buell, S.; Rutledge, G. C.; Van Vliet, K. J. *ACS. Appl. Mater. Interfaces.* **2010**, 2, 1164.

180. Vatankhah, E.; Semnani, D.; Prabhakaran, M. P.; Tadayon, M.; Razavi, S.; Ramakrishna, S. *Acta. Biomater.* **2014**, 10, 709.

List of figures

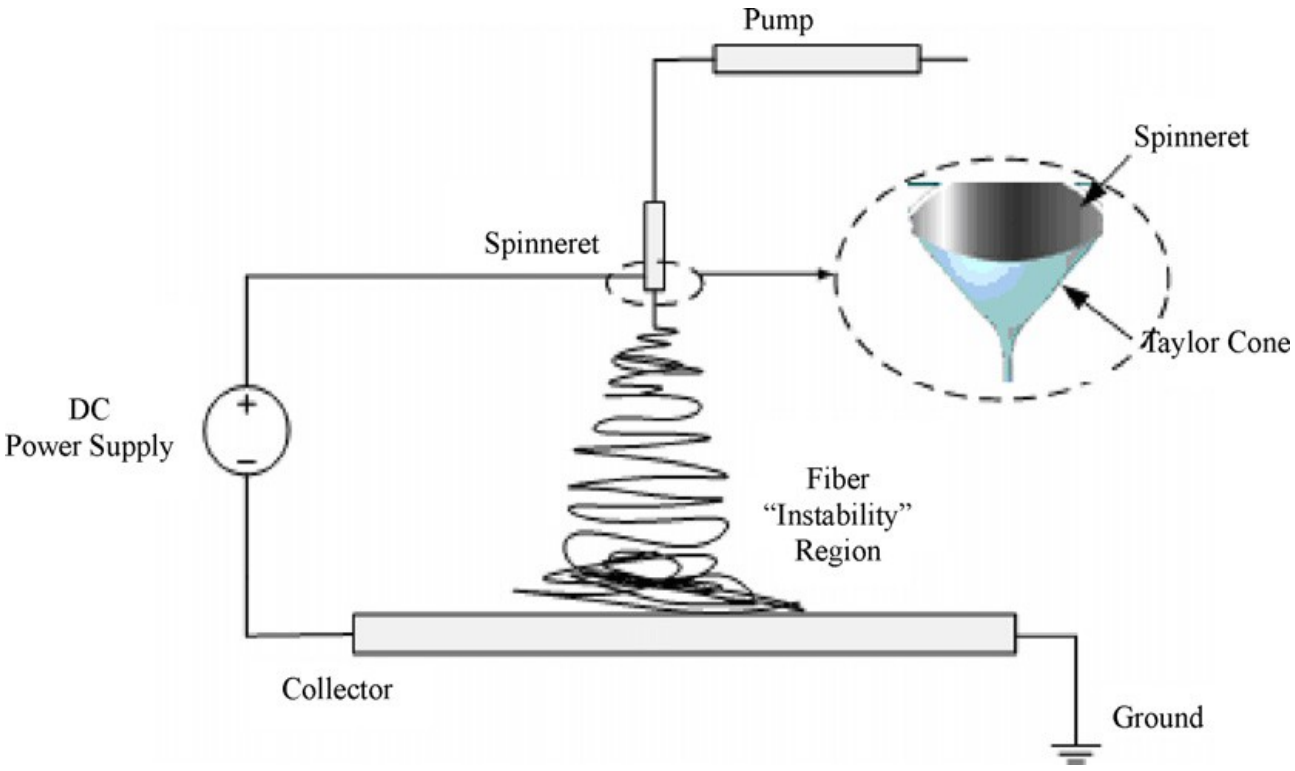
Pump
Spinneret
Spinneret
Taylor Cone
DC
Power Supply
Fiber
"Instability"
Region
Collector
Ground

Figure 1

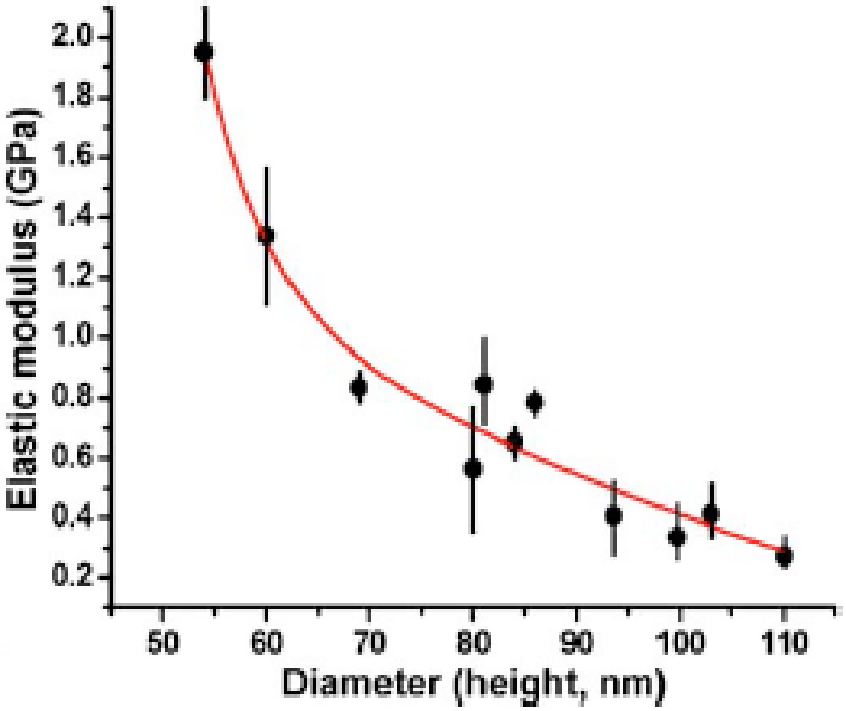
Elastic modulus (GPa)
2.0
1.8
1.6
1.4
1.2
1.0
0.8
0.6
0.4
0.2
50
60
70
80
90
100
110
Diameter (height, nm)

Figure 2

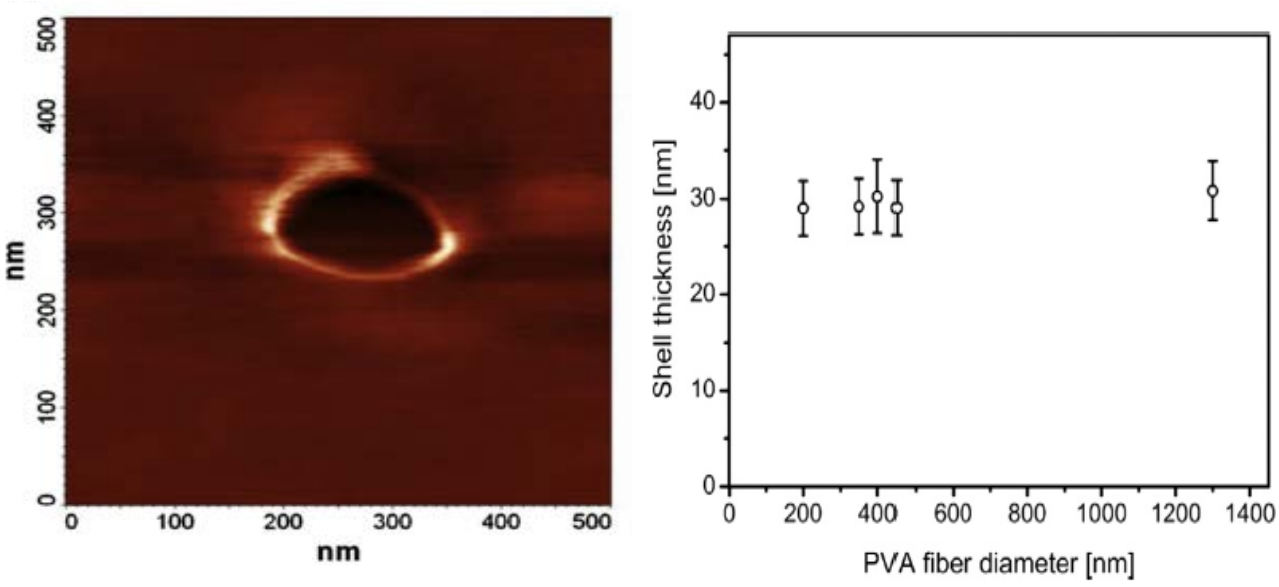
nm
0
100
200
300
400
500
nm
Shell thickness [nm]
0
10
20
30
40
0
200
400
600
800
1000
1200
1400
PVA fiber diameter [nm]

(a) **(b)**

Figure 3

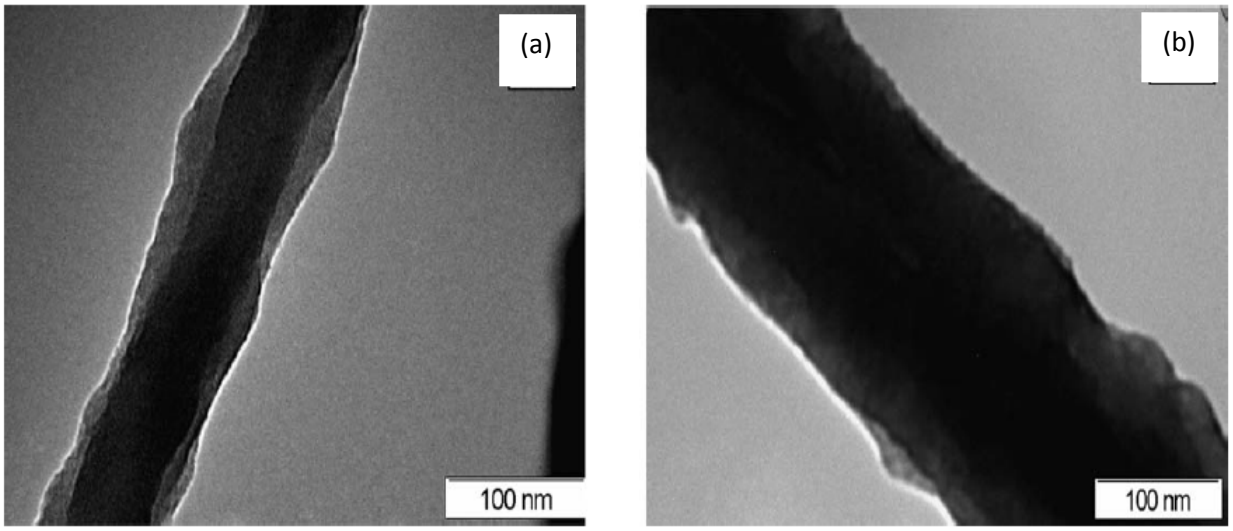

Figure 4

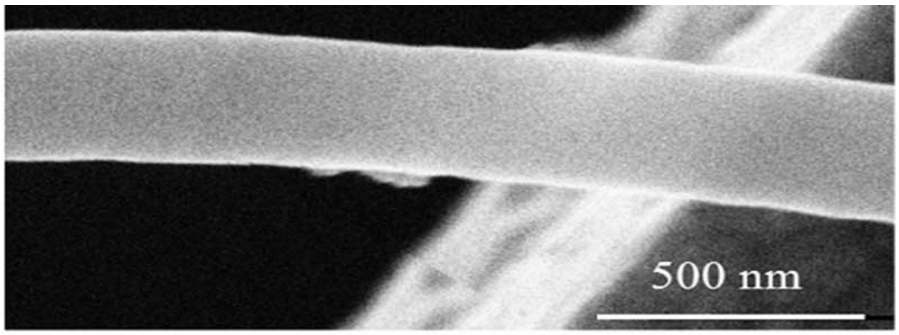

(a) Undeformed fiber

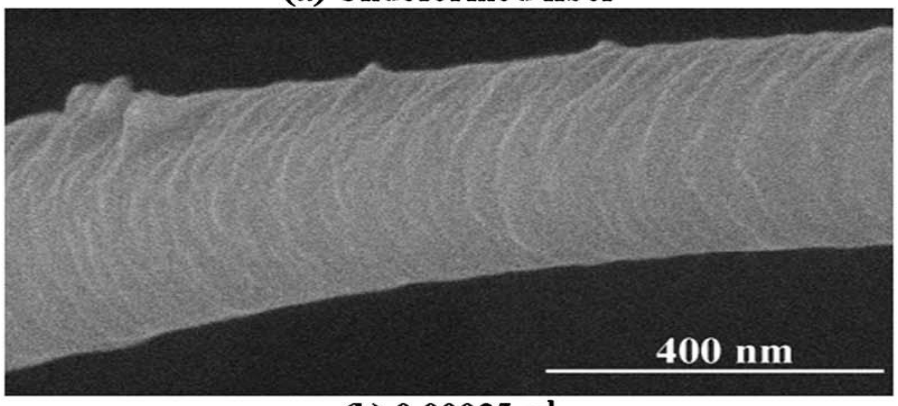

(b) 0.00025 s^{-1}

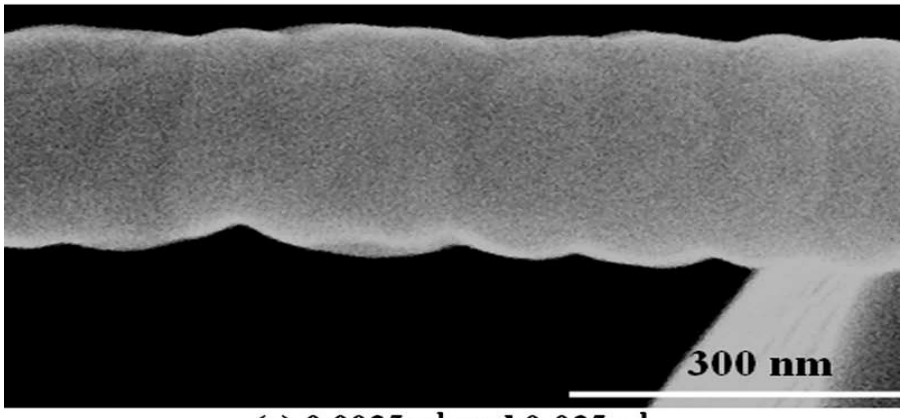

(c) 0.0025 s^{-1} and 0.025 s^{-1}

Figure 5

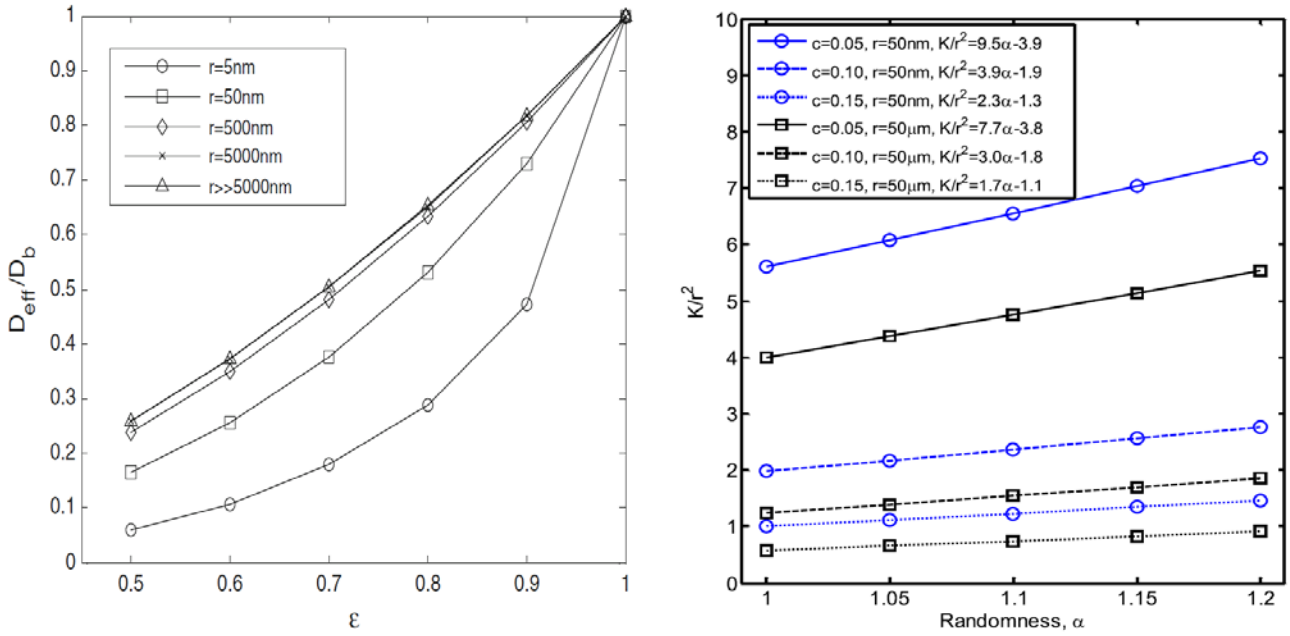
r=5nm
r=50nm
r=500nm
r=5000nm
r>>5000nm
D_{eff}/D_b
ε
c=0.05, r=50nm, K/r²=9.5α-3.9
c=0.10, r=50nm, K/r²=3.9α-1.9
c=0.15, r=50nm, K/r²=2.3α-1.3
c=0.05, r=50μm, K/r²=7.7α-3.8
c=0.10, r=50μm, K/r²=3.0α-1.8
c=0.15, r=50μm, K/r²=1.7α-1.1
K/r²
Randomness, α

(a) **(b)**

Figure 6

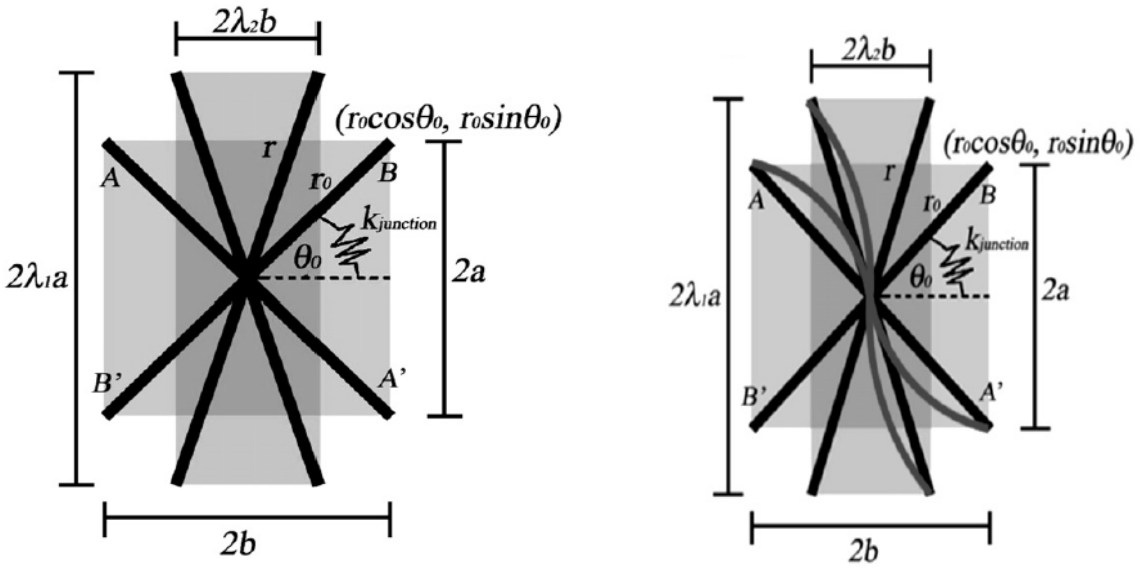
2λ2b
(r0cosθ0, r0sinθ0)
r
A
r0
B
kjunction
θ0
2λ1a
2a
B'
A'
2b
2λ2b
(r0cosθ0, r0sinθ0)
r
A
r0
B
kjunction
θ0
2λ1a
2a
B'
A'
2b

(a) **(b)**

Figure 7

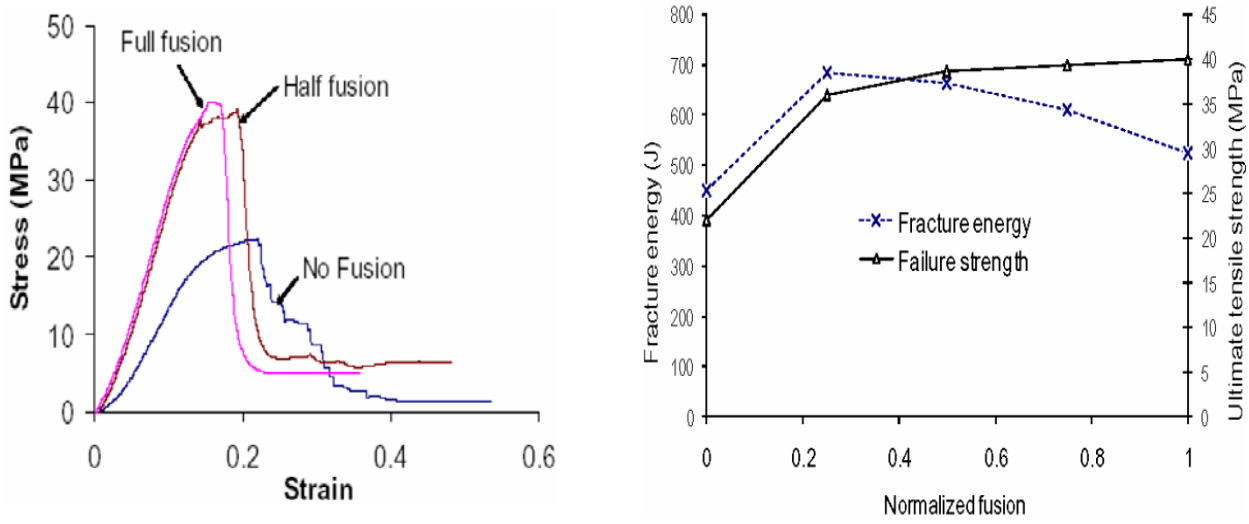
Full fusion
Half fusion
No Fusion
Stress (MPa)
Strain
0
10
20
30
40
50
0
0.2
0.4
0.6
Fracture energy
Failure strength
Fracture energy (J)
Ultimate tensile strength (MPa)
Normalized fusion
0
100
200
300
400
500
600
700
800
0
5
10
15
20
25
30
35
40
45
0
0.2
0.4
0.6
0.8
1

(a) **(b)**

Figure 8

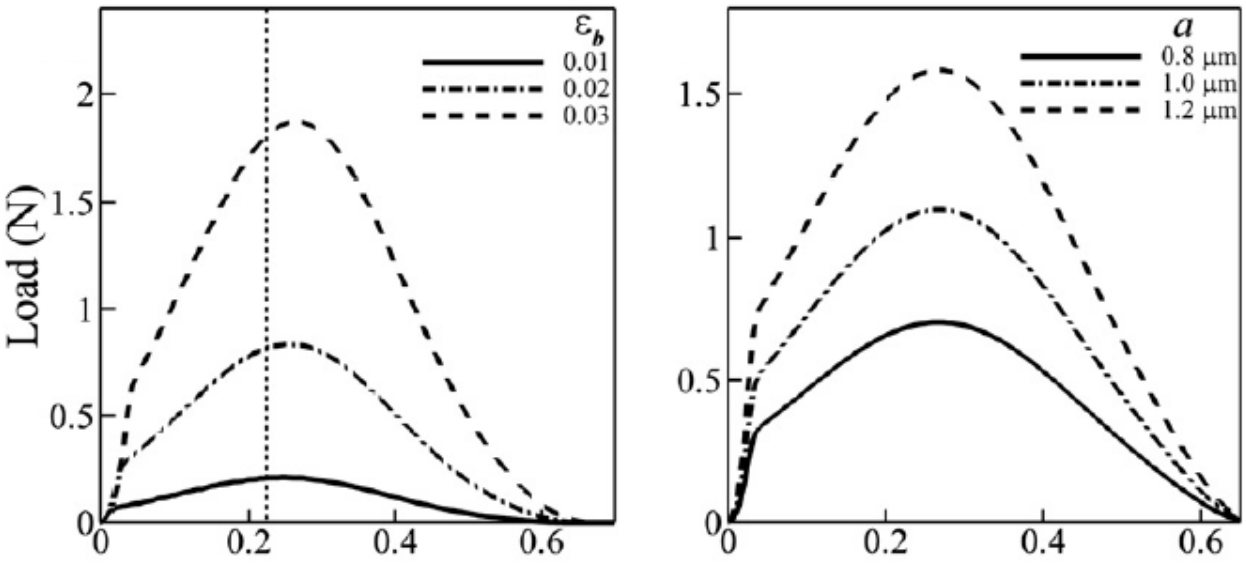
Load (N)
ε_b
0.01
0.02
0.03
2
1.5
1
0.5
0
0
0.2
0.4
0.6
a
0.8 μm
1.0 μm
1.2 μm
1.5
1
0.5
0
0
0.2
0.4
0.6
Displacement ΔL (cm)

(a) **(b)**

Figure 9

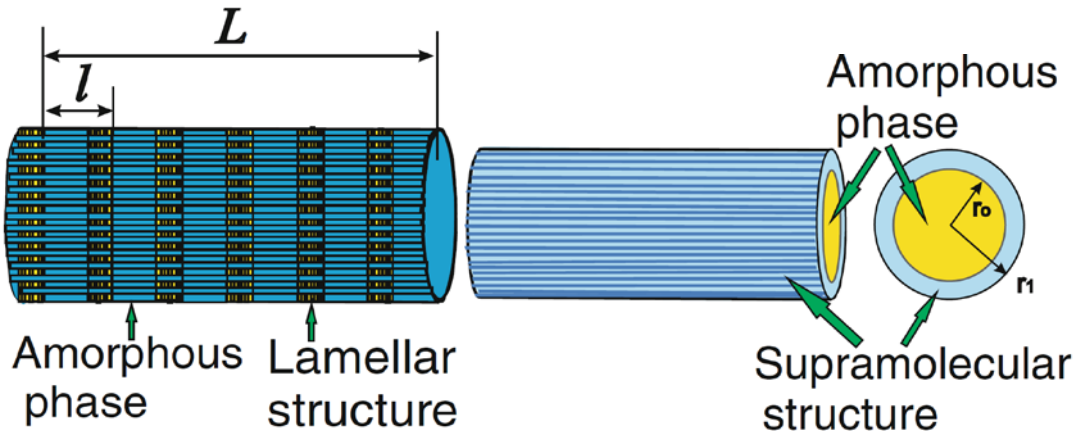
L
l
Amorphous phase
Lamellar structure
Amorphous phase
r0
r1
Supramolecular structure

(a) **(b)**

Figure 10

Table 1: Modelling different electrospun nanofibres by using RSM and ANN methods.

Nanofibre	Modelling method	Input parameter	Output parameter	Reference
poly(D,L-lactide)	RSM	Solution concentration and applied voltage	Fibre diameter and its standard deviation	[112]
PVA	RSM	Solution concentration, spinning distance, applied voltage and flow rate	Fibre diameter and its standard deviation	[96]
Ferrofluid/PVA	RSM	Flow rate, applied voltage, spinning distance and collector rotating speed	Fibre diameter and its standard deviation	[116]
Polyacrylonitrile	RSM	Solution concentration and applied voltage	Fibre diameter	[108]
	RSM	Solution concentration, applied voltage and flow rate	Fibre diameter, fibre alignment and ultimate tensile load	[110]
	RSM	Solution concentration, applied voltage and spinning distance	Fibre diameter and its standard deviation	[109]
	RSM	Berry's number, charge density spinneret diameter, spinning angle, collector size and charge density	Fibre diameter and its standard deviation	[117]
	ANN	Relative humidity, temperature, flow rate, spinning distance, applied voltage, electric field, weight percent of PAN in polymer solution, solution viscosity, electrical conductivity and surface tension		[114]
	RSM and ANN	Solution concentration, applied voltage and spinning distance		[113]
Poly (L-lactide)	RSM	Solution concentration, applied voltage, Take-up rate and spinning distance	Fibre diameter, yarn diameter, strength and modulus	[118]

PVDF	RSM	solvent mixing ratio, field strength and mass fraction of PVDF	Fibre diameter	[119]
Polyvinylacetate	RSM	Solution concentration and applied voltage	Fibre diameter	[120]
Gelatin	ANN	Applied voltage, temperature, polymer concentration and solvent concentration	Fibre diameter	[121]
Gelatin/Chitosan	RSM	Gelatin/chitosan blend ratio, applied voltage, flow rate	Fibre diameter	[122]
Gelatin/ glycosaminoglycan (GAG)	RSM	Applied voltage, feed rate, gelatin/GAG blend ratio	Fibre diameter and its standard deviation	[123]
Gelatin/PCL	RSM	Gelatin concentration, PCL concentration, acetic acid content in overall solvents and gelatin solution content in the blend solution	Fibre diameter	[103]
Chitosan /PVA	RSM	Solution concentration, spinning distance and applied voltage	Fibre diameter	[124]
		Applied voltage and flow rate	Fibre diameter	[125]
Chitosan/hydroxyapatite	RSM	Spinning distance, applied voltage and flow rate	Fibre diameter	[126]
Chitosan/ polylactide	RSM	Applied voltage and flow rate	Fibre diameter and its standard deviation	[127]
Cellulose acetate	RSM	Spinning distance, applied voltage and feed rate	Fibre diameter	[128]
Chitosan	RSM	Solution concentration, applied voltage and ratio of solvents	Fibre diameter	[129]
Silk	RSM	Solution concentration and applied voltage	Fibre diameter and its Standard deviation	[130]
		Solution concentration, applied voltage and spinning distance	Fibre diameter	[111]
PMMA	RSM	Solution concentration, spinning distance,	Fibre diameter	[131]

		temperature, flow rate and applied voltage		
	RSM and ANN	Solution concentration, spinning distance and flow rate	Fibre diameter	[115]
Poly[(butylene succinate)-co-(butylene adipate)]/clay		Solution concentration and clay loading	Fibre diameter and its standard deviation	[132]
	RSM	Solution concentration, clay loading and flow rate	Fibre diameter, Bead diameter, bead number and surface density	[133]
Zein	RSM	Solution concentration, applied voltage, spinning distance and flow rate	Fibre diameter	[106]
Titanium dioxide	RSM	Solution concentration, applied voltage, spinning distance, flow rate and pH value	Fibre diameter	[134]
		Polyvinylpyrrolidone content and titanium tetraisopropoxide content	Fibre diameter	[104]
		Applied voltage, flow rate and spinning distance		
PCL	RSM	Needle diameter, solution concentration and field strength	Fibre diameter	[105]
polyamide 6	RSM	Solution concentration, spinning distance, flow rate and applied voltage	Fibre diameter	[135]
Starch	RSM	Solution concentration, spinning distance and applied voltage	Fibre diameter	[136]
PEO	ANN	Solution concentration, eectrical conductivity, flow rate and applied voltage	Fibre diameter	[27]
	ANN	PEO concentration, acetic acid	Fibre diameter	[137]

		concentration, applied voltage and temperature		
Polyurethane (PU)	RSM and ANN	Solution concentration, spinning distance and applied voltage	Fibre diameter	[138]
Nylon-6,6	ANN	Solution concentration, flow rate, spinning distance and applied voltage,	Fibre diameter	[139]